Supporting information for "Nano-mole Scale Signal Assignment by [1]H Detected Protein Solid-state NMR by Ultra-Fast Magic-Angle Spinning and HIGHLIGHT Spectral Editing"

by Songlin Wang, Sudhakar Parthasarathy, Yiling Xiao, Yusuke Nishiyama, Fei Long, Isamu Matsuda, Yuki Endo, Takahiro Nemoto, Kazuo Yamauchi, Tetsuo Asakura, Mitsuhiro Takeda, Tsutomu Terauchi, Masatsune Kainosho, and Yoshitaka Ishii[*]

Experimental Details

All the multi-dimensional NMR data were processed using the nmrPipe software.[1] Unless stated otherwise, all indirect time-domain signals in the 2D and 3D data were extended to 1.5-fold and 2-fold by linear prediction, respectively. The multi-dimensional SSNMR data were apodized with 45°- and 60°-shifted sine-bell window functions in the ^{1}H and ^{13}C/^{15}N dimensions, respectively, to balance sensitivity and resolution. The cooling N_2 gas temperature was set to -20°C, and the temperature of the GB1 sample was approximately 30°C. The pulse sequences and experimental conditions are shown in the supplementary figures and their captions below.

Preparation of lysine reverse labeled GB1 microcrystals

E. coli BL21 (DE3) cells transformed with a pET3 vector encoding GB1 T2Q mutant were grown in 500 mL of M9 medium enriched with 2.0 g/L of ^{13}C$_6$-D-glucose and 1.0 g/L of ^{15}NH$_4$Cl at 37 °C using New Brunswick Scientific EXCELLA E24R incubator until OD$_{600}$ reached ~0.8. At this time, 3.0 mM of unlabeled L-Lys was additionally supplemented for 0.5 h. The GB1 expression was induced by adding 0.8 mM isopropyl-β-D-thiogalactopyranoside. After 4 h of the induction, the cells were harvested. Harvested cells were suspended in a 5-mL PBS buffer (1.7 mM KH$_2$PO$_4$, 5 mM Na$_2$HPO$_4$, 150 mM NaCl, pH 7.4) per gram of cells, heated at 80 °C for exactly five minutes, then immediately cooled on ice for 10 minutes. The cell lysate was centrifuged using a Sorvall Lynx 6000 centrifuge (Thermo Scientific) at 3.06×10^4 g for 30 min at 4 °C. The supernatant was dialyzed against a 50 mM sodium phosphate buffer (pH 5.6, 0.02 w/v% NaN$_3$), and then the protein was purified by HPLC. GB1 eluted when the acetonitrile concentration is approximately 50% (v/v). The collected fraction was dialyzed in a 50 mM sodium phosphate buffer (pH 5.6) containing NaN$_3$ (0.02 w/v% NaN$_3$) for a buffer exchange.[2]

For preparation of microcrystalline GB1 used for SSNMR, we first concentrated the protein in the 50 mM sodium phosphate buffer to ~30 mg/mL by ultrafiltration. The GB1 solution was concentrated in an Amicon Ultra-4 centrifugal filter (Ultracel-3; 3-kDa molecular-weight cutoff; EMD Millipore) using an Eppendorf 5810R centrifuge at 6.0×10^3 g and 4 °C in a 15-mL conical tube. The concentrated GB1 solution (~500 μL) recovered from the filter unit was mixed with a crystallization solution (a 1:2 (v/v) mixture of 2-propanol and (+/–)-2-methyl-2,4-pentanediol; Hampton Research) in a 1:3 (v/v) ratio. The crystallization solution was added to the protein solution in three aliquots so that the final concentration becomes 75% (v/v) crystallization solution and 25% (v/v) protein solution.[3] The solution was mixed well after each addition of the crystallization solution. GB1 was crystallized for 30 min at room temperature.

A solution containing microcrystals (~2 mL) was centrifuged in a micro-centrifuge tube using a Sorvall Legend Micro 17 centrifuge at 6.0×10^3 g for ~3 min in order to sediment the crystals. Then, a supernatant (~1.9 mL) was removed from the test tube. Subsequently, Cu-EDTA (Ethylenediaminetetraacetoc acid copper(II) disodium salt, Sigma-Aldrich) was dissolved into the supernatant and vortexed. The Cu-EDTA solution of ~1.9 mL was introduced to the microcrystals so that the final Cu-EDTA concentration was 20 mM. Doping of Cu-EDTA was employed to suppress ^{1}H T_1 values of the protein sample. Cautions should be exercised as Cu-EDTA also reduces ^{1}H T_2 values in a concentration dependent manner. Thus, doping of excess Cu-EDTA may introduce line broadening for the residues exposed to the protein surface,[4] although no notable ^{1}H line broadening was observed in the condition used for our experiments. The mechanism of a paramagnetic relaxation for the PACC experiments under UFMAS conditions is not well understood. A further analysis is needed in order to quantitatively examine the relaxation dynamics under UFMAS.

The principle of HIGHLIGHT spectral editing

We briefly explain the principle of HIGHLIGHT spectral editing using the pulse sequence in Fig. S1 used to collect the data in Fig. 1b. ^{15}N spin polarization was prepared with double-quantum adiabatic cross polarization (DQ-CP)[4, 5] using an amplitude-modulated shaped pulse for the ^{15}N channel and a rectangular pulse for the ^{1}H channel. The DQ-CP scheme was

adjusted so that the sum of the average RF nutation frequencies for the ^{1}H and ^{15}N channels (ω_H + $<\omega_N>$)/2π was matched to the spinning frequency of ω_R/2π,[5] where ω_A/2π denotes an RF nutation frequency in the CP scheme for nuclei A (A = ^{1}H or ^{15}N) and $<\omega_A>$ denotes its time average. During the HIGHLIGHT mixing, a π-pulse train with the XY-16 phase cycle was rotor-synchronously applied in n rotor cycles to the ^{13}C channel so that two π-pulses were applied in one rotor cycle. This scheme reintroduces heteronuclear dipolar couplings between ^{15}N and ^{13}C. This π-pulse train is followed by a refocusing scheme by a Gaussian selective pulse on ^{13}CO and a hard ^{15}N π-pulse and the second set of the XY16 π-pulse train on the ^{13}C channel. This set of the pulse sequence corresponds a frequency selective REDOR scheme[6] that allows for reintroducing dipolar couplings only between ^{15}N and ^{13}CO; hence, the ^{15}N signals do not decay due to a strong dipolar coupling between ^{15}N and ^{13}C$_\alpha$ within a residue. The frequency selective REDOR sequence is repeated m times (m = 2 in Fig. S1-3). The effective mixing time of ($2nm\tau_R$) should be experimentally adjusted by changing n and m so that a ^{15}N signal for a residue next to a labeled ^{13}CO is nearly completely dephased while a ^{15}N signal for the "highlighted" residue following an unlabeled residue is not dephased by two-bond ^{15}N–^{13}CO dipolar coupling within the same residue. It should be noted that the dephasing curve does not follow that for a standard REDOR sequence as the RF duty factor for the π-pulse train is close to 1.0. We empirically found that the sequence with m of 2 performed better than that with m of 1 for the total effective mixing time used in our experiments. After the HIGHLIGHT mixing, ^{15}N shifts are recorded in the t_1 period. The ^{15}N polarization is transferred to amide ^{1}H for signal detection after a water suppression scheme. A resulting spectrum exhibits ^{15}N–^{1}H correlations only for the residues following selective unlabeled residues in a reverse-labeled protein in which residues other than the selected amino-acid types are uniformly ^{13}C and ^{15}N-labeled. Further details and simulation results of the HIGHLIGHT mixing at varied spinning speeds will be presented in our forthcoming paper.
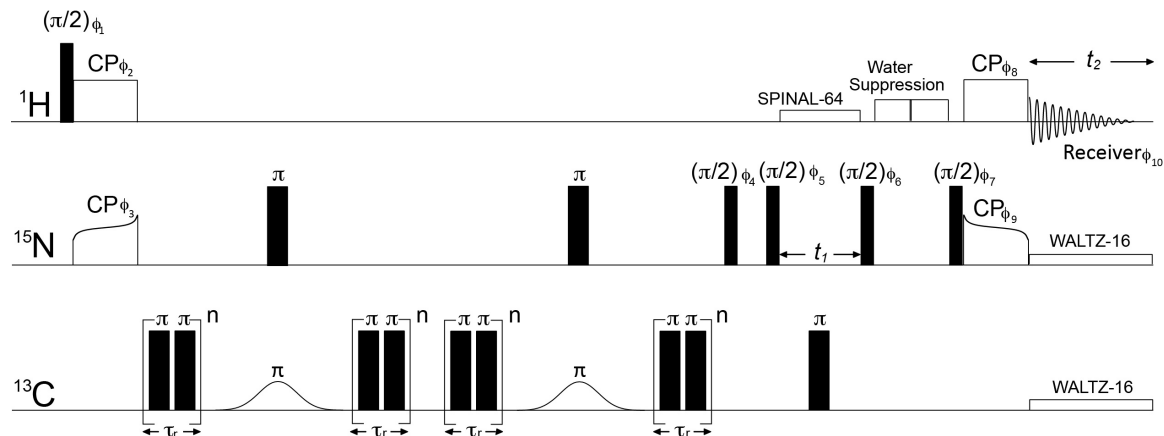
Supplementary Figure

Figure S1. The pulse sequence for the 2D ^{15}N/^{1}H correlation experiment with a HIGHLIGHT REDOR scheme used for Fig. 1b. The control experiment in Fig. 1a was performed with the sequence without the mixing period (i.e. $n = 0$). ^{15}N spin polarization was prepared with double-quantum adiabatic cross polarization (DQ-CP) using an amplitude-modulated shaped pulse with an upward tangential ramp for the ^{15}N channel and a rectangular pulse for the ^{1}H channel. The ^{15}N RF field strength was ramped from 17.2 kHz to 28.7 kHz with the average rf field at $\sim 2\nu_R/7$ while the ^{1}H RF field amplitude was kept constant at 58 kHz ($\sim 5\nu_R/7$). The contact time of the first CP was 1.25 ms. Then, ^{15}N signals were dephased for directly bonded ^{15}N-^{13}CO pairs by the HIGHLIGHT REDOR sequence without ^{1}H rf irradiation. During the HIGHLIGHT REDOR mixing, a π-pulse train with the XY-16 phase cycle was rotor-synchronously applied to the ^{13}C channel so that two π-pulses were applied in one rotor cycle. The π-pulse width was 6.0 μs and $n = 72$. A Gaussian shape π-pulse with the maximum rf strength of 5k Hz and a pulse width of 265 μs was applied to selectively invert the carbonyl ^{13}C spin states. Then, the second π-pulse train to ^{13}C was applied. The mixing scheme was repeated twice. After the HIGHLIGHT REDOR mixing, a transverse component of the ^{15}N polarization was stored along the z-axis and the unnecessary coherences were dephased during a z-filter period of 5 ms. After the excitation by a $\pi/2$-pulse, the ^{15}N chemical shift was recorded during the t_1 period with an t_1 increment of 0.45 ms and the maximum t_1 period of 16.2 ms. During the t_1 period, SPINAL-64 ^{1}H decoupling was applied with RF field strengths of 10 kHz and a ^{13}C π-pulse was applied at the middle of t_1 for ^{13}C-^{15}N decoupling. Then, a selected transverse component of the ^{15}N polarization was stored along the z-axis. During the z-filter period, two water-suppression pulses of 2-ms widths and 19.5-kHz field strength were applied. The ^{15}N polarization was transferred back to ^{1}H spins by an adiabatic CP scheme for ^{1}H detection in the t_2 period. The contact time of the second CP period was 0.7 ms. .^{1}H chemical shifts were recorded during the t_2 period under 10 kHz WALTZ-16 ^{13}C decoupling and 2 kHz WALTZ-16 ^{15}N decoupling. The t_2 acquisition time was 6.4 ms with 5 μs dwell time. The phase cycles for the pulse sequence were as follows: $\phi_1 = $ y; $\phi_2 = $ x; $\phi_3 = $ x, x, -x, -x; $\phi_4 = $ y; $\phi_5 = $ -y; $\phi_6 = $ y, y, y, y, -y, -y, -y, -y; $\phi_7 = $ x; $\phi_8 = $ x; $\phi_9 = $ y, -y; $\phi_{10} = $ x, -x, -x, x, -x, x, x, -x. The phase ϕ_5 and the receiver phase were incremented along the t_1 points using the States-TPPI data collection mode.
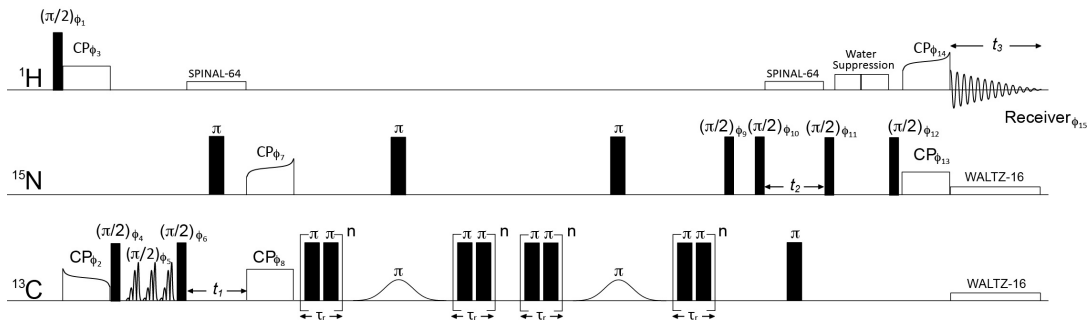
Figure S2. The pulse sequence for the 2D CA(N)H and 3D CANH correlation experiments with the HIGHLIGHT REDOR scheme used for Fig. 1c, Fig. 2, and Fig. 4a. For the 2D version used for Fig. 1c, the t_2 value was set to 0.1 µs and t_3 was incremented as t_2. Standard 3D CANH experiments without HIGHLIGHT REDOR in Fig. 1c (blue) were performed using this sequence without the mixing period (i.e. $n = 0$ for Fig.1c. $n = 0$ and Gaussian π-pulses on ^{13}C channel was removed for Fig.2 and Fig.4). ^{13}C spin polarization was prepared with adiabatic double-quantum cross polarization (DQ-CP) using an amplitude-modulated shaped pulse with a downward tangential ramp for the ^{13}C channel and a rectangular pulse for the ^{1}H channel. The ^{13}C RF field strength was ramped down from 76.3 kHz to 45.8 kHz, and the ^{1}H RF field strength was kept constant at 16.0 kHz. The contact time of the first CP was 1.5ms. To saturate unwanted ^{13}CO polarization, three E-BURP-2 shaped π/2-pulses were applied near the ^{13}CO resonance (175 ppm) before the t_1 period. For each E-burp pulse, the maximum field strength was 11.0 kHz and the pulse width was 0.3 ms. After the t_1 period, the ^{13}C polarization was transferred to ^{15}N spins by applying the adiabatic DQ-CP with an upward tangential ramp for ^{15}N. During the contact time of 6.0 ms, the ^{15}N RF field was ramped from 16.6 kHz to 27.6 kHz while the ^{13}C RF field was kept at 57.3 kHz. Then, ^{15}N signals were quenched by the HIGHLIGHT REDOR sequence without ^{1}H rf irradiation. After the HIGHLIGHT mixing, a transverse component of the ^{15}N polarization was stored along the z-axis, and the unnecessary coherences were removed during the z-filter period of 5 ms. During the t_1 and t_2 period, SPINAL-64 ^{1}H decoupling was applied with RF field strengths of 10 kHz. One ^{15}N π-pulse and one ^{13}C π-pulse decoupling were applied at the middle of t_1 and t_2 respectively. A water suppression pulse was applied after t_2 as discussed in Fig.S6. Then, the ^{15}N polarization was transferred back to ^{1}H spins by adiabatic DQ-CP for ^{1}H detection in the t_3 period. In the DQ-CP sequence, the ^{1}H RF field was ramped from 35.4 kHz to 59.0 kHz and the ^{15}N RF field strength was set constant to 27.2 kHz. The contact time of the third DQ-CP period was 0.7 ms. ^{1}H chemical shifts are recorded during the t_3 period under 10 kHz WALTZ-16 ^{13}C decoupling and 5 kHz WALTZ-16 ^{15}N decoupling. For Fig. 1c, the t_1 increment was 0.2 ms. For Fig. 2, the t_1 increment was 0.2 ms, the t_2 increment was 0.45 ms. For Fig. 4, the t_1 increment was 0.25 ms, and the t_2 increment was 0.425 ms. The phase cycles were as follows: $\phi_1 = $ y; $\phi_2 = $ x, -x; $\phi_3 = $ x; $\phi_4 = $ x ; $\phi_8 = $x; $\phi_7 = $ x, x −x, -x; $\phi_9 = $ y; $\phi_{10} = $ -y; $\phi_{12} = $ x; $\phi_{11} = $ x, x, x, x, -x, -x, -x, -x; $\phi_{13} = $ x, -x, -x, x, -x, x, x, -x. $\phi_1 = $ y; $\phi_2 = $ x, -x; $\phi_3 = $ x; $\phi_4 = $ y; $\phi_5 = $ y; $\phi_6 = $ y; $\phi_7 = $ x, x −x, -x; $\phi_8 = $ x; $\phi_9 = $ y; $\phi_{10} = $ -y; $\phi_{11} = $ y; $\phi_{12} = $ -y; $\phi_{13} = $ x, x, x, x, -x, -x, -x, -x; $\phi_{14} = $ x; $\phi_{15} = $ x, -x, -x, x, -x, x, x, -x. The phase ϕ_6, ϕ_{10} and the receiver phase were incremented along the t_1 and t_2 points using the States-TPPI mode.
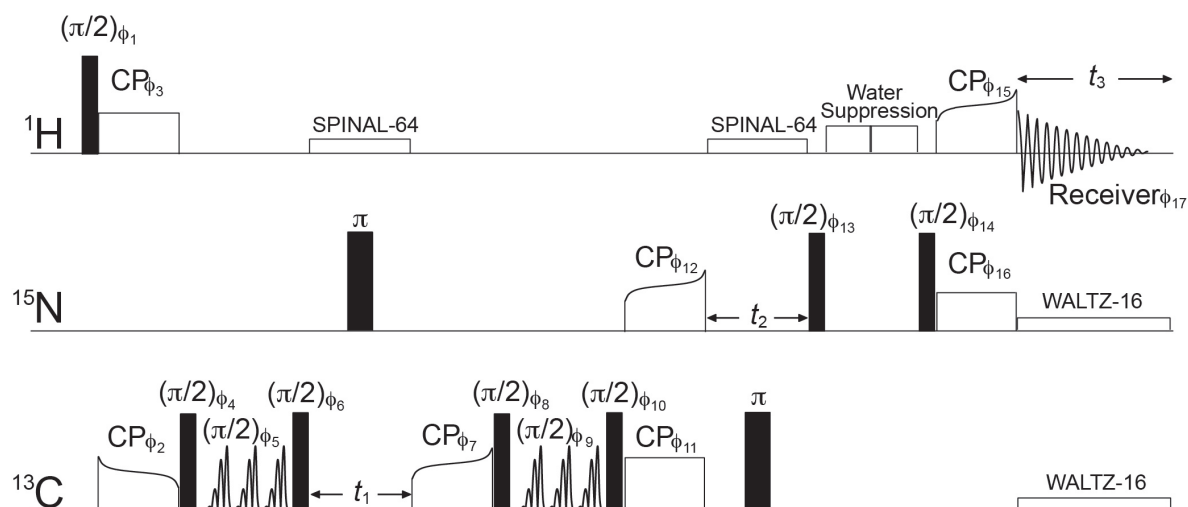
Figure S3. The pulse sequence for the 3D CA(CO)NH correlation experiment used for Fig. 2. ^{13}C spin polarization was prepared with adiabatic double-quantum cross polarization (DQ-CP) using an amplitude-modulated shaped pulse with a downward tangential ramp for the ^{13}C channel and a rectangular pulse for the ^{1}H channel. The ^{13}C RF field strength ramped down from 76.3 kHz to 45.8 kHz, and the ^{1}H RF field strength was set to 16.0 kHz. The contact time of the first CP was 1.5ms. As discussed in Fig. S2, three E-Burp $\pi/2$-pulses were applied to selectively dephase unwanted ^{13}CO polarization after the CP period. After the t_1 period, the ^{13}C$_\alpha$ polarization was transferred to carbonyl ^{13}C by using a DREAM sequence[7] with an upward tangential ramp from 26.3 kHz to 43.8 kHz. Another set of selective E-burp pulses were applied near the ^{13}C$_\alpha$ resonance (50 ppm) before the t_2 period to selectively dephase unwanted ^{13}C$_\alpha$ polarization. Then, the ^{13}C polarization was transferred to ^{15}N by adiabatic DQ-CP with an upward tangential ramp for the ^{15}N channel and a rectangular pulse for the ^{13}C channel. The ^{15}N RF field amplitude ramped from 16.2 kHz to 27.0 kHz and the ^{13}C RF field amplitude was set to 58.0 kHz. The contact time of the ^{13}C-^{15}N DQ-CP was 6.0 ms. The rest of the pulse sequence was the same as that in Fig.S2. The t_1 increment was 0.2 ms, the t_2 increment was 0.45 ms, and the t_3 acquisition time was 7.2ms with 0.5 µs dwell time. The phase cycles for the pulse sequence were as follows: ϕ_1 = y; ϕ_2 = x, -x; ϕ_3 = x; ϕ_4 = y; ϕ_5 = y; ϕ_6 = y; ϕ_7 = x; ϕ_8 = y; ϕ_9 = y; ϕ_{10} = y; ϕ_{11} = x; ϕ_{12} = x, x, -x, -x; ϕ_{13} = y; ϕ_{14} = -y; ϕ_{15} = x; ϕ_{16}= x, x, x, x, -x, -x, -x, -x; ϕ_{17} = x, -x, -x, x, -x, x, x, -x. The phase ϕ_6, ϕ_{12} and the receiver phase were incremented along the t_1 and t_2 points using the States-TPPI data collection mode.
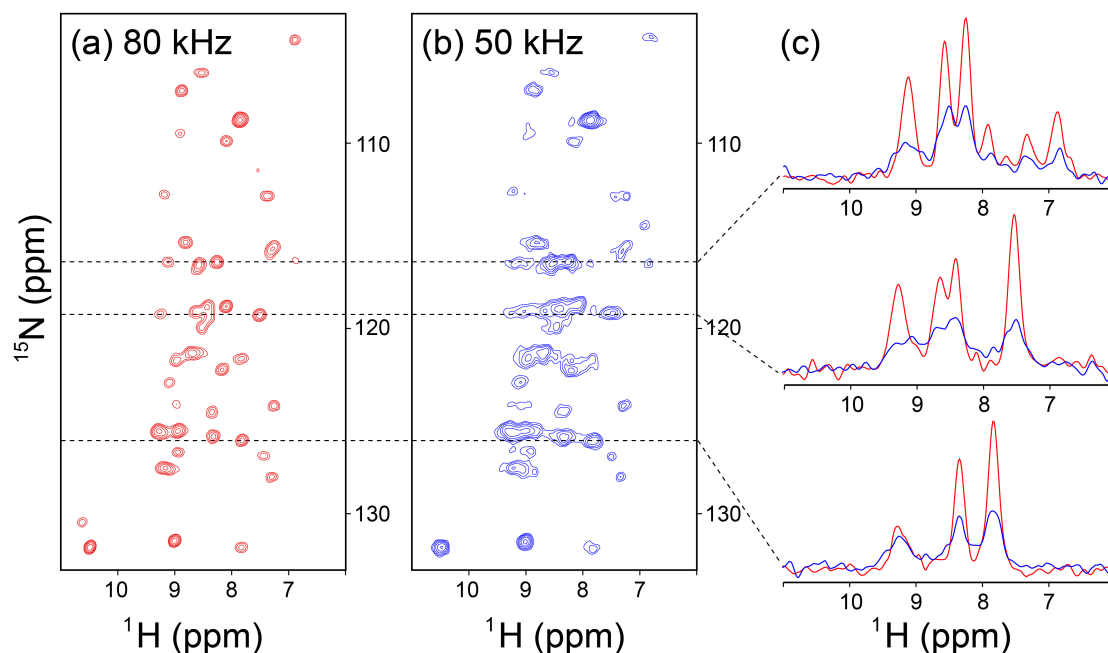
Figure S4. A comparison of 2D ^{15}N/^{1}H correlation spectra of the same lysine-reverse-labeled GB1 microcrystal sample collected under MAS at (a) 80 kHz and (b) 50 kHz. The pulse sequence is comprised by two adiabatic CP schemes with all the contact times of 1.5 ms. The spin polarization was transferred from ^{1}H to ^{15}N by the first adiabatic CP; then the ^{15}N signal was monitored in the t_1 period. After the t_1 period, the polarization was transferred back from ^{15}N to ^{1}H spins by the second adiabatic CP scheme for ^{1}H detection. For the data in (a), during the first adiabatic CP period, the ^{15}N RF field strength was ramped up from 18.6 kHz to 31.0 kHz with the average rf field at ~ν_R/3 while the ^{1}H RF field was kept constant at 55 kHz (~$2\nu_R$/3). For the second adiabatic CP period, the ^{15}N RF field was ramped down from 33.3 kHz to 19.9 kHz with the average rf field at ~ν_R/3 while the ^{1}H RF field was kept at 55 kHz (~$2\nu_R$/3). For the data in (b), during the first adiabatic CP period, the ^{15}N RF field was ramped from 10.6 kHz to 17.7 kHz with the average rf field at ~$2\nu_R$/7, while the ^{1}H RF field strength was kept at 35 kHz (~$5\nu_R$/7). In the second adiabatic CP period, the ^{15}N RF field was ramped from 9.7 kHz to 16.1 kHz with the average rf field at ~ν_R/4 while the ^{1}H RF field amplitude was kept at 37 kHz (~$3\nu_R$/4). The cooling N$_2$ gas temperature was set to -18°C for experiment under 80 kHz spinning and 18°C for experiment under 50 kHz spinning so that the GB1 sample temperature was approximately 30°C for the both cases. The data were collected with 16 scans for each t_1 period; the recycle delay was set as 0.2 s and the total experimental time was 4.5 min for each spinning condition. (c) 1D slices of the 2D NH spectra for the spinning speeds of 80 kHz (red) and 50 kHz (blue). For a comparison of the sensitivity and resolution, the slices are displayed in the same scale.
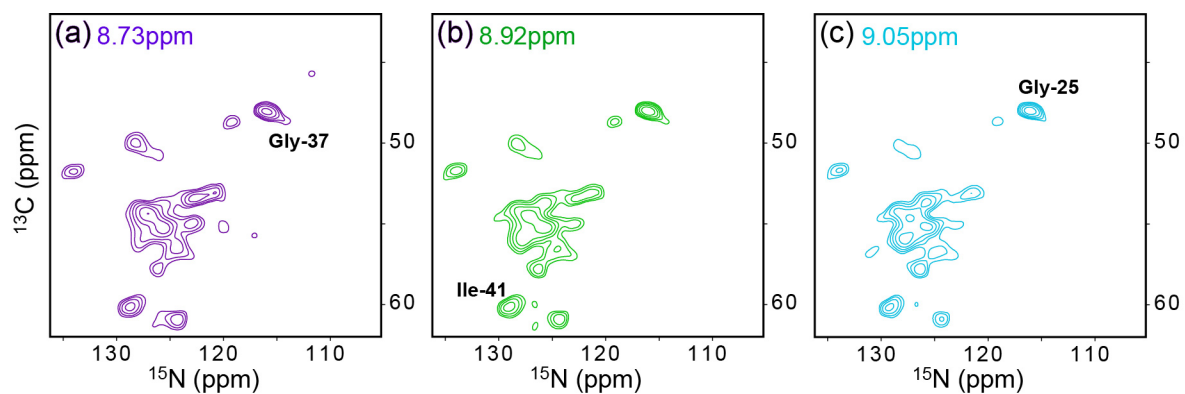
Figure S5. Three color-coded 2D $^{13}C_{\alpha}/^{15}N$ slices from the 3D CANH spectrum of Aβ(1-42) fibrils at the ^{1}H shift positions indicated in the inset. The corresponding 2D projection is displayed in Fig. 4b. The pulse sequence and experimental condition of 3D CANH experiment were described in Fig. S2.

Table S1. The signal assignments of the lysine-reverse-labeled GB1 microcrystalline sample.

	^{15}N	^{13}CO	$^{13}C_\alpha$	$^{13}C_\beta$	^1H
M1	-	171.4	54.4	-	-
Q2	125.7	174.7	55.9	30.7	8.2
Y3	123.9	-	57.3	43.2	8.95
K4	-	-	-	-	-
L5	127.3	174.9	53.2	42.7	9.02
I6	126.8	175.1	60.2	37.8	8.95
L7	127.4	175	54.8	42.7	9.18
N8	125.5[d]	176.8	51.1	38.5	8.92[d]
G9	109.5	-	44.8	-	8.04
K10	-	-	-	-	-
T11	107.4	173.2	62.2	69.5	8.82
L12	127.3	-	54.6	43.7	7.18
K13	–	-	-	-	-
G14	106.4	171.1	45.3	-	8.54
E15	121.5	174	54.1	33.8	8.74
T16	115.5	172	60.6	70.6	8.8
T17	116	174.3	60.4	72.8	8.25
T18	116.2	171.5	61.9	70.9	9.13
E19	126	175.7	55	31.2	7.89
A20	124.7[d]	177.4	51.1	23.2	9.16[d]
V21	116.5	174.8	64	32	8.41
D22	115.7	*	53.3	*	7.37
A23	*	*	*	*	-
A24	121.6	181.4	54.9	*	7.96
T25	117.4	175.8	67.6	*	8.38
A26	124	177.2	55.2	17.4	7.28
E27	117	-	59.5	28.9	8.58
K28	-	-	-	-	-
V29	118.9	178.3	66.6	31.7	7.54
F30	119.1	-	57.5	37.5	8.61
K31	-	-	-	-	-
Q32	121.3	177.5	59.1	28.7	7.8
Y33	121	178.4	61.6	38.8	8.54
A34	122.7	179.6	56.2	18	9.07
N35	118.8	179.5	57.3	40	8.48

D36	121.7	176.2	56.3	38.3	8.97
N37	115.4	174.3	53.8	40.6	7.31
G38	108.5	174	47.2	-	7.89
V39	122.3	175	62.1	31.9	8.18
D40	130.8	175.2	53.6	*	8.87
G41	108.3	172.7	45.5	-	7.8
E42	120.1	177.6	55.5	31.1	8.54
W43	125.5	176.8	57.7	33.4	8.9
T44	109.6	173.8	61.1	73.1	9.03
Y45	119.5	171.9	57.9	42.8	9.26
D46	126.9	176.3	51.2	42.8	7.47
D47	125.9	177.3	*	*	8.67
A48	119.5	179.2	54.3	18.8	8.28
T49	104.2	-	60.8	70.1	6.95
K50	-	-	-	-	-
T51	113.1	174.3	62.8	71.6	7.44
F52	130.1	175.7	56.7	43.2	10.56
T53	113.4	172.2	60.8	71.7	9.22
V54	119.3	172.7	58.7	32.6	8.12
T55	124.3	173.9	61.3	72.1	8.35
E56	132.2	-	*	*	7.82

a) The main-chain assignments were obtained by 3D CANH, CA(CO)NH, CONH experiments. Additionally, 3D CX(CA)NH experiment was performed for $^{13}C_{\beta}$ assignments. All chemical shifts were calibrated based on DSS standard.

b) The peaks noted by * were missing in the 3D spectra presumably due to higher mobility.

c) The peaks noted by – were not observed by the 3D experiments because of the reverse labeling, because the site does not exist ($^{13}C_{\beta}$ Gly), or because the residue was located at the terminus.

d) Assignments of these resonances required 3D CX(CA)NH in addition to 3D CANH and 3D CA(CO)NH experiments. All other ^{15}N, $^{13}C_{\alpha}$, ^{1}H resonances could be assigned solely from the 3D CANH and 3D CA(CO)NH experiments.

Table S2. The torsion angles of the lysine-reverse-labeled GB1 microcrystalline sample predicted by TALOS+ software and corresponding angles from an X-ray structure.

	Torsion angles predicted from ^{1}H, ^{13}C$_\alpha$, ^{13}CO, ^{13}C$_\beta$, ^{15}N [b] (φ, ψ)	Torsion angles predicted from ^{1}H, ^{13}C$_\alpha$, ^{15}N [b] (φ, ψ)	X-ray torsion angles[8] (φ, ψ)
M1			
Q2	(-99±24, 137±13)	(-103±21, 136±16)	(-83, 132)
Y3	(-121±13, 145±15)	(-117±17, 142±16)	(-120, 146)
K4	(-119±10, 130±13)	(-107±18, 125±9)	(-118, 144)
L5	(-103±9, 123±17)	(-112±13, 126±13)	(-118, 126)
I6	(-109±15, 123±12)	(-120±10, 126±8)	(-98, 121)
L7	(-104±13, 119±19)	(-106±13, 127±16)	(-98, 121)
N8	(-108±27, 129±33)[# a]	(-131±21, 120±51)[#]	(-132, 58)
G9	(-173±85, 170±29)[#]	(-, -)[#]	(-78, 172)
K10	(-74±80, 166±46)[#]	(-60±13, -28±18)[#]	(-58, -42)
T11	(-105±17, 1±12)	(-107±17, 0±16)	(-122, -20)
L12	(-120±35, 135±20)[#]	(-113±35, 131±42)[#]	(-98, 118)
K13	(-137±16, 162±14)	(-108±37, 155±14)[#]	(-133, 157)
G14	(-169±53, 161±22)[#]	(81±8, 9±13)[#]	(130, -146)
E15	(-135±16, 143±16)	(-69±74, 142±47)[#]	(-145, 149)
T16	(-120±24, 145±17)	(-139±6, 147±11)	(-144, 158)
T17	(-120±21, 151±11)	(-132±20, 149±14)	(-126, 157)
T18	(-126±23, 130±14)	(-112±26, 134±11)	(-142, 150)
E19	(-113±17, 124±6)	(-129±20, 126±31)[#]	(-95, 120)
A20	(-123±39, 153±14)	(-85±18, 163±26)[#]	(-143, 157)
V21	(-70±13, -27±10)	(-70±20, -17±17)	(-72, -25)
D22	(-105±13, -2±20)[#]	(-102±19, -5±13)[#]	(-163, 170)
A23	(-71±26, -32±26)	(-67±20, -42±11)	(-69, -33)
A24	(-65±6, -41±4)	(-61±3, -39±3)	(-64, -37)
T25	(-66±4, -41±6)	(-66±5, -46±4)	(-72, -43)
A26	(-63±5, -44±7)	(-61±5, -45±7)	(-59, -39)
E27	(-63±5, -39±6)	(-65±5, -38±4)	(-57, -44)
K28	(-65±5, -40±5)	(-68±7, -32±19)	(-63, -45)
V29	(-62±11, -44±4)	(-64±11, -42±4)	(-59, -50)
F30	(-70±11, -29±17)	(-66±11, -38±17)	(-68, -40)
K31	(-69±14, -39±16)	(-81±22, -22±35)	(-68, -36)
Q32	(-62±5, -44±6)	(-64±6, -45±6)	(-65, -44)
Y33	(-64±5, -42±8)	(-64±5, -41±7)	(-59, -47)
A34	(-63±4, -41±6)	(-64±4, -39±5)	(-62, -49)

N35	(-62±4, -41±6)	(-63±4, -41±5)	(-57, -45)
D36	(-62±4, -26±9)	(-64±5, -28±11)	(-68, -24)
N37	(-94±12, 4±9)	(-92±16, 5±10)	(-100, 14)
G38	(86±8, 12±11)	(78±10, 20±14)[#]	(75, 20)
V39	(-80±16, 132±8)	(-95±20, 127±10)	(-93, 122)
D40	(-111±23, 130±25)	(-113±31, 127±25)	(-127, 92)
G41	(177±58, 177±19)[#]	(-173±60, 171±32)[#]	(-139, -172)
E42	(-102±16, 126±16)	(-118±33, 138±16)	(-96, 144)
W43	(-103±11, 144±13)	(-104±21, 156±7)	(-119, 143)
T44	(-130±23, 154±12)	(-135±28, 160±5)	(-124, 162)
Y45	(-144±16, 129±17)	(-125±22, 129±14)	(-146, 131)
D46	(-116±21, 134±29)	(-111±10, 124±32)	(-116, 114)
D47	(-68±22, -23±26)	(-59±4, -32±10)	(-71, -17)
A48	(-69±12, -26±12)	(-70±10, -22±12)	(-80, -36)
T49	(-102±17, -4±15)	(-110±10, -6±24)	(-106, 2)
K50	(65±6, 24±13)[#]	(-77±7, -13±12)[#]	(56, 37)
T51	(-115±25, 131±8)	(-114±22, 127±8)	(-123, 129)
F52	(-117±17, 150±10)	(-106±17, 136±28)	(-101, 150)
T53	(-134±11, 147±10)	(-126±15, 148±143)	(-131, 147)
V54	(-126±18, 132±14)	(-132±9, 135±12)	(-132, 132)
T55	(-98±16, 117±13)	(-92±24, 126 ±16)	(-134, 130)
E56			

a) The torsion angles noted by # were categorized as "ambiguous" prediction by the TALOS+ software (Ver 3.40 F1 Rev 2011.030.18.13).

b) The predicted torsion angles highlighted by yellow show deviations exceeding 15° and the indicated error from the angles obtained by the X-ray structure.

Supplementary References:

1. F. Delaglio, S. Grzesiek, G. W. Vuister, G. Zhu, J. Pfeifer and A. Bax, *J. Biomol. NMR*, 1995, **6**, 277-293.
2. J. M. Louis, I. J. L. Byeon, U. Baxal and A. M. Gronenborn, *J. Mol. Biol.*, 2005, **348**, 687-698.
3. W. T. Franks, D. H. Zhou, B. J. Wylie, B. G. Money, D. T. Graesser, H. L. Frericks, G. Sahota and C. M. Rienstra, *J. Am. Chem. Soc.*, 2005, **127**, 12291-12305.
4. N. P. Wickramasinghe, S. Parthasarathy, C. R. Jones, C. Bhardwaj, F. Long, M. Kotecha, S. Mehboob, L. W. M. Fung, J. Past, A. Samoson and Y. Ishii, *Nature Methods*, 2009, **6**, 215-218.
5. S. Parathasarathy, Y. Nishiyama and Y. Ishii, *Acc. Chem. Res.*, 2013, **46**, 2127-2135.
6. C. P. Jaroniec, B. A. Tounge, J. Herzfeld and R. G. Griffin, *J. Am. Chem. Soc.*, 2001, **123**, 3507-3519.
7. R. Verel, M. Ernst and B. H. Meier, *J. Magn. Reson.*, 2001, **150**, 81-99.
8. H. L. F. Schmidt, L. J. Sperling, Y. G. Gao, B. J. Wylie, J. M. Boettcher, S. R. Wilson and C. A. Rienstra, *J. Phys. Chem. B*, 2007, **111**, 14362-14369.